Solvent Dependence of the Structure and Magnetic Ordering of Ferrimagnetic Manganese(III) *meso*-Tetraphenylporphyrin Tetracyanoethenide, $[MnTPP]^{+}[TCNE]^{\bullet-}\cdot x$(solvent). Evidence for Orientationally Disordered $[TCNE]^{\bullet-}$

Wendy Hibbs,[1a] Durrell K. Rittenberg,[1a] Ken-ichi Sugiura,[1a,b] Brian M. Burkhart,[1c,d] Brian G. Morin,[1d,e] Atta M. Arif,[1a] Louise Liable-Sands,[1f] Arnold L. Rheingold,[1f] Muttaiya Sundaralingam,[1c] Arthur J. Epstein,[1c,e] and Joel S. Miller*[,1a]

Department of Chemistry, University of Utah, 315 S. 1400 E., Room 2020, Salt Lake City, Utah 84112-0850, Department of Chemistry and Department of Physics, The Ohio State University, Columbus, Ohio 43210-1106, and Department of Chemistry, University of Delaware, Newark, Delaware 19716

Received October 31, 2000

Tetraphenylporphinatomanganate(III) tetracyanoethenide, [MnTPP][TCNE], is the prototype of a growing family of linear chain (1-D) coordination polymers that magnetically order as ferrimagnets. [MnTPP][TCNE]·*x*S [S = PhMe ($x = 2$), 1,2-$C_6H_4Me_2$ ($x = 1$), 1,2-$C_6H_4Cl_2$ ($x = 3$), 1,2,4-$C_6H_3Cl_3$ ($x = 2$), and 1,3-$C_6H_4Cl_2$ ($x = 2$)] have been prepared and structurally and magnetically characterized. All form 1-D chain structures with intrachain Mn···Mn separations ranging from 9.202 to 10.218 Å. The 173 K crystal structure of [MnTPP][TCNE]·2PhMe has been rerefined, revealing that the $[TCNE]^{\bullet-}$ is 2-fold-disordered and coordinated to Mn^{III} by a pair of trans cyano nitrogen atoms to form parallel one-dimensional chains. The two orientations of $[TCNE]^{\bullet-}$ are related by a 180° rotation about the diagonal axis joining the trans nitrogen atoms bound to Mn^{III}. The major form has an occupancy of 83.3(4)% with a $Mn-N_{TCNE}$ distance of 2.328(3) Å and a MnNC angle of 146.8(8)°. The minor form, with 16.7(4)% occupancy, has a $Mn-N_{TCNE}$ distance of 2.176(15) Å and a MnNC angle of 152.3(39)°. Lattice packing and molecular bonding imply static as opposed to dynamic disorder. The magnetic properties depend on the type and quantity of the solvent present in the structure. Desolvation via heating in *n*-octane (127 °C), *n*-dodecane (216 °C), and/or vacuum thermolysis (175 °C) leads to numerous different desolvated materials with differing magnetic properties. At higher temperatures the magnetic susceptibility can be fit by the Curie−Weiss expression, $\chi \propto (T - \theta)^{-1}$, with $\theta = 44$, 52, 72, 55, and 77 K for the toluene, 1,2-xylene, 1,2-dichlorobenzene, 1,3-dichlorobenzene, and 1,2,4-trichlorobenzene solvates, respectively. The T_c's were taken as the maximum in 10 Hz $\chi'(T)$ and are 7.8, 9.2, 11.3, 10.8, and 8.2 K for the PhMe, 1,2-xylene, 1,2-dichlorobenzene, 1,3-dichlorobenzene, and 1,2,4-trichlorobenzene solvates, respectively. Upon desolvation the T_c's increase for the PhMe, 1,2-xylene, 1,2,4-trichlorobenzene solvates and decrease for the 1,2- and 1,3-dichlorobenezene solvates. The compounds show one-dimensional ferrimagnetic exchange behavior at high temperatures with intrachain exchange of $J/k_b = -63$, -99, -234, -100, and -200 K for toluene, 1,2-xylene, 1,2-dichlorobenzene, 1,3-dichlorobenzene, and 1,2,4-trichlorobenzene solvates, respectively, as determined from fits to the Seiden expression, which models isolated 1-D interactions among alternating $S = 2$ classical and $S = {}^1/_2$ quantum spins. For variation in the temperature at which the peak occurs per decade of frequency, ϕ, $(\Delta T_f/T_f)/\Delta(\log \omega)$ is 0.167, 0.168, 0.066, 0.171, and 0.024 for toluene, 1,2-xylene, 1,2-dichlorobenzene, 1,3-dichlorobenzene, and 1,2,4-trichlorobenzene, respectively, typical of spin glass behavior. Since $[TCNE]^{\bullet-}$ is only disordered for the PhMe solvate and all five solvates exhibit spin glass behavior, the spin glass behavior cannot be attributed to this disorder.

Introduction

The study of magnetically ordered molecule-based materials is a growing area of contemporary chemistry, and establishment of structure−function relationships is critical to its advancement.[2,3] $[Fe(C_5Me_5)_2]^{\bullet+}[TCNE]^{\bullet-}$ (TCNE = tetracyanoethylene) was the first organic-containing molecule-based magnet characterized and has an ordering temperature T_c of 4.8 K.[4] Improvements led to the discovery of $V(TCNE)_x\cdot y$(solvent), the first room-temperature organic magnet ($T_c \approx 400$ K),[5] and later the magnetically ordered Mn, Fe, Ni, and Co analogues.[6] More recently, studies have focused on a class of metallomacrocycle/$[TCNE]^{\bullet-}$-based magnets exemplified by [MnTPP][TCNE]·2PhMe, **1a** (H_2TPP = *meso*-tetraphenylporphyin).[3a,7,8] **1a** was first predicted to consist of π/π $[TCNE]^{\bullet-}/[MnTPP]^{+}$ interactions,[9] akin to $[Fe(C_5Me_5)_2][TCNE]$;[4b] however, the structure

(1) (a) University of Utah. (b) Current address: Osaka University. (c) Department of Chemistry, The Ohio State University. (d) Current address: Milliken Research Corporation, Spartanburg, SC 29304. (e) Department of Physics, The Ohio State University. (f) University of Delaware.

(2) (a) *Proceedings of the Conference on Ferromagnetic and High Spin Molecular Based Materials*; Miller, J. S., Dougherty, D. A., Eds.; Molecular Crystals and Liquid Crystals 176; Gordon and Breach Science: New York, 1989. (b) *Proceedings of the Conference on Molecular Magnetic Materials*; Gatteschi, D., Kahn, O., Miller, J. S., Palacio, F., Eds.; NATO ARW Molecular Magnetic Materials; Kluwer Academic: Dordrecht, 1991; *E198*. (c) *Proceedings of the Conference on* the *Chemistry and Physics of Molecular Based Magnetic Materials*; Iwamura, H., Miller, J. S., Eds.; Molecular Crystals and Liquid Crystals 232/233; Gordon and Breach Science: New York, **1993**, *232/233*. (d) *Proceedings of the Conference on Molecule-based Magnets*; Miller, J. S., Epstein, A. J., Eds.; Molecular Crystals and Liquid Crystals 271−274; Gordon and Breach Science: New York, 1995. (e) *Proceedings of the Conference on Molecular-Based Magnets*; Itoh, K., Miller, J. S., Takui, T., Eds.; Molecular Crystals and Liquid Crystals 305/306; Gordon and Breach Science: New York, 1997. (f) Turnbull, M. M., Sugimoto, T., Thompson, L. K., Eds.; *American Chemical Society Symposium Series*; American Chemical Society: Washington, DC, 1996; Vol. 644. (g) *Proceedings of the 6th Conference on Molecular-Based Magnets*; Kahn, O., Ed.; Molecular Crystals and Liquid Crystals 334/335; Gordon and Breach Science: New York, 1999.

10.1021/ic0011922 CCC: $20.00
Published on Web 03/13/2001

determination[7a] revealed that $S = {}^1/_2$ $[TCNE]^{\bullet-}$ is trans-μ-*N*-σ-bound to $S = 2$ Mn^{III} forming 1-D $\cdots D^+A^{\bullet-}D^+A^{\bullet-}\cdots$ (D = MnTPP; A = TCNE) chains. This material is a ferrimagnet with a critical temperature T_c of 18 K, as determined by extrapolating the maximum slope of the low-field $M(T)$ curve to $M = 0$.[7b,8] More recently, it is common to report T_c as the maximum in the real component of the low-frequency (10 Hz) ac susceptibility.[3a] Further study of **1a** revealed signs of complicated magnetic dynamics suggestive of disorder that was not evident in the crystal structure.[10]

During the study of **1a**, numerous other solvates as well as their desolvated forms were prepared and studied. These included [MnTPP][TCNE]·*x*S [S = PhMe, **1a** ($x = 2$); 1,2-$C_6H_4Me_2$, **1b** ($x = 1$); 1,2-$C_6H_4Cl_2$, **1c** ($x = 3$); 1,3-$C_6H_4Cl_2$, **1d** ($x = 2$); and, 1,2,4-$C_6H_3Cl_3$, **1e** ($x = 2$)], where *x* is determined from single-crystal X-ray analyses and is the number of solvates when all solvent sites in the unit cell are fully occupied. Herein, we report the structural and magnetic consequences arising from these solvent substitutions as well as from desolvation for this family of magnets.

Experimental Section

Synthesis. All manipulations involving $[TCNE]^{\bullet-}$ were carried out under nitrogen using standard Schlenck techniques or in a Vacuum Atmospheres DriLab. Solvents used for the preparation of the $[TCNE]^{\bullet-}$ salts were predried and distilled from appropriate drying agents. H_2TPP was prepared according to the Alder−Longo method.[11a] [Mn^{III}TPP][OAc] complexes were prepared from H_2TPP and $Mn(OAc)_2\cdot 4H_2O$;[11b] the $Mn(OAc)_2\cdot 4H_2O$ was predissolved in *N*,*N*-dimethylformamide (DMF) and filtered before addition to the free-base porphyrin, to remove paramagnetic impurities. The [Mn^{III}TPP][OAc] salts were subsequently reduced to Mn^{II}TPP as Mn^{II}TPP(py) (py = pyridine) by $NaBH_4$, utilizing a literature method.[11b] TCNE was obtained as a gift from O. Webster and was sublimed prior to use. [MnTPP][TCNE]·*x*S (S = solvent) was prepared according to the general method as reported by Summerville et al. with the exception that the material was not dried in vacuo as described.[9] All physical measurements of solvated materials were performed immediately after collecting the shiny black crystals on a glass frit in order to minimize solvent loss.

Table 1. Infrared TCNE Stretching Data for [MnTPP][TCNE]·*x*S

	ν_{CN}, cm^{-1} (m)			ν_{CN}, cm^{-1} (s)		
compound	solvated	α	β	solvated	α	β
$[TCNE]^0$ [15]	2259			2221		
$[Fe(C_5Me_5)_2]^{\bullet+}[TCNE]^{\bullet-}$ [4b,a]	2183			2143		
$[TCNE]^{2-}$ [15]	2104			2069		
1a·2PhMe	2195	2192	2192	2148	2147	2147
1b·1,2-$C_6H_4Me_2$	2193	2191	2192	2131	2134	2134
1c·3(1,2-$C_6H_4Cl_2$)	2196	2193	2192	2132	2135	2133
1d·2(1,3-$C_6H_4Cl_2$)	2200	2193	2193	2129	2135	2134
1e·2(1,2,4-$C_6H_3Cl_3$)	2195	2193	2192	2136	2135	2135

[a] Unbound $[TCNE]^{\bullet-}$.

Desolvation was effected by either vacuum thermolysis (α method) of freshly prepared **1** in a glass vial heated in a tube furnace under dynamic vacuum at 175 °C for 12 h or by heating freshly prepared **1** (ca. 25 mg) to reflux (β method) in 7 mL of either *n*-octane (bp = 127 °C) (β_o) or *n*-dodecane (bp = 216 °C) (β_d) for 10 min followed by filtering the hot mixture through a medium glass-frit funnel and collecting the insoluble desolvated **1**. Complete desolvation was confirmed by thermogravimetric analysis−mass spectroscopy (TGA/MS).

[MnTPP][TCNE]·*x*PhMe, 1a, was prepared as previously reported by reaction of Mn^{II}TPPpy and TCNE in toluene; however, the sample was not dried until α and β desolvation.[9] IR (cm^{-1}) at room temperature: 2195 (m), 2148 (s) for ν_{CN}. TGA/MS: 17.9% weight loss at 108.5 °C corresponding to $x = 1.88$. **1a** was thermally annealed according to the α and β_o methods, and the ν_{CN} IR data are reported in Table 1.

[MnTPP][TCNE]·*x*(1,2-$C_6H_4Me_2$), 1b, was prepared as described above using 80.3 mg (0.11 mmol) of Mn^{II}TPPpy and 51.2 mg (0.40 mmol) of TCNE, both dissolved in 10 mL of boiling *o*-xylene and filtered before addition. IR (cm^{-1}) at room temperature: 2193 (m), 2131 (s) for ν_{CN}. Anal. Calcd (obsd) for [MnTPP][TCNE]·1,2-$C_6H_4Me_2$ [$C_{58}H_{38}N_8Mn$]: C 77.24 (77.43%), H 4.25 (4.51%), N 12.43 (12.27%). TGA/MS: 13.93% weight loss at 164 °C corresponding to $x = 1.04$. Desolvation was performed according to the α and β_d methods, and the ν_{CN} IR data are reported in Table 1.

[MnTPP][TCNE]·*x*(1,2-$C_6H_4Cl_2$), 1c, was prepared as described above using 80.8 mg (0.11 mmol) of Mn^{II}TPPpy and 28.0 mg (0.22 mmol) of TCNE, both dissolved in 10 mL of boiling *o*-dichlorobenzene and filtered before addition. IR (cm^{-1}) at room temperature: 2196 (m), 2132 (s) for ν_{CN}. Anal. Calcd (obsd) for [MnTPP][TCNE]·2.28(1,2-$C_6H_4Cl_2$) [$C_{63.675}H_{37.125}Cl_{4.56}N_8Mn$]: C 67.64 (67.74%), H 3.31 (3.58%), N 9.91 (9.67%). TGA/MS: 32.23% weight loss at 153 °C corresponding to $x = 2.17$. Desolvation was performed according to the α and β_o methods, and the ν_{CN} IR data are reported in Table 1.

[MnTPP][TCNE]·*x*(1,3-$C_6H_4Cl_2$), 1d, was prepared as described above using 96.8 mg (0.13 mmol) of Mn^{II}TPPpy and 55.3 mg (0.43 mmol) of TCNE, both dissolved in 10 mL of boiling *m*-dichlorobenzene and filtered before addition. IR (cm^{-1}) at room temperature: 2200 (w), 2129 (s) for ν_{CN}. Calcd (obsd) for [MnTPP][TCNE]·2(1,3-$C_6H_4Cl_2$) [$C_{62}H_{36}Cl_4N_8Mn$]: C 68.33 (68.35%), H 3.33 (3.44%), N 10.28 (10.31%). TGA/MS: 27.43% weight loss at 123 °C corresponding to

(3) Reviews. (a) Miller, J. S.; Epstein, A. J. *Chem. Commun.* **1998**, 1319. (b) Ovcharenko, V. I.; Sagdeev, R. Z. *Russ. Chem. Rev.* **1999**, *68*, 345. (c) Plass, W. *Chem.−Ztg.* **1998**, *32*, 323. (d) Miller, J. S.; Epstein, A. J. *Chem. Eng. News* **1995**, *73* (40), 30. (e) Miller, J. S.; Epstein, A. J. *Angew. Chem., Int. Ed. Engl.* **1994**, *33*, 385. (f) Kinoshita, M. *Jpn. J. Appl. Phys.* **1994**, *33*, 5718. (g) Miller, J. S.; Epstein, A. J. *Adv. Chem. Ser.* **1995**, *245*, 161. (h) Caneschi, A.; Gatteschi, D. *Progr. Inorg. Chem.* **1991**, *37*, 331. (i) Buchachenko, A. L. *Russ. Chem. Rev.* **1990**, *59*, 307. (j) Kahn, O. *Struct. Bonding* **1987**, *68*, 89. (k) Caneschi, A.; Gatteschi, D.; Sessoli, R.; Rey, P. *Acc. Chem. Res.* **1989**, *22*, 392. (l) Gatteschi, D. *Adv. Mater.* **1994**, *6*, 635. (m) Miller, J. S.; Epstein, A. J.; Reiff, W. M. *Acc. Chem. Res.* **1988**, *21*, 114. (n) Miller, J. S.; Epstein, A. J.; Reiff, W. M. *Science* **1988**, *240*, 40. (o) Miller, J. S.; Epstein, A. J.; Reiff, W. M. *Chem. Rev.* **1988**, *88*, 201. (p) Miller, J. S.; Epstein, A. J. In *New Aspects of Organic Chemistry*; Yoshida, Z., Shiba, T., Oshiro, Y., Eds.; VCH Publishers: New York, 1989; Vol. 237. (q) Kahn, O. *Molecular Magnetism*; VCH Publishers: New York, 1993.

(4) (a) Miller, J. S.; Calabrese, J. C.; Epstein, A. J.; Bigelow, R. W.; Zhang, J. H.; Reiff, W. M. *J. Chem. Soc., Chem. Commun.* **1986**, 1026. (b) Miller, J. S.; Calabrese, J. C.; Rommelmann, H.; Chittipeddi, S.; Zhang, J. H.; Reiff, W. M.; Epstein, A. J. *J. Am. Chem. Soc.* **1987**, *109*, 769.

(5) (a) Manriquez, J. M.; Yee, G. T.; McLean, R. S.; Epstein, A. J.; Miller, J. S. *Science* **1991**, *252*, 1415. (b) Epstein, A. J.; Miller, J. S. In *Conjugated Polymers and Related Materials: The Interconnection of Chemical and Electronic Structure*, Proceedings of Nobel Symposium NS-81; Oxford University Press: Oxford, U.K., 1993; p 475. *Chim. Ind.* **1993**, *75*, 185, 257. (c) Miller, J. S.; Yee, G. T.; Manriquez, J. M.; Epstein, A. J. In *Conjugated Polymers and Related Materials: The Interconnection of Chemical and Electronic Structure*, Proceedings of Nobel Symposium NS-81; Oxford University Press: Oxford, U.K., 1993; p 461. *Chim. Ind.* **1992**, *74*, 845.

(6) Zhang, J. H.; Ensling, J.; Ksenofontov, V.; Gütlich, P.; Epstein, A. J.; Miller, J. S. *Angew. Chem., Int. Ed.* **1998**, *37*, 657.

(7) (a) Miller, J. S.; Calabrese, J. C.; McLean, R. S.; Epstein, A. J. *Adv. Mater.* **1992**, *4*, 498. (b) Zhou, P.; Morin, B. G.; Epstein, A. J.; McLean, R. S.; Miller, J. S. *J. Appl. Phys.* **1993**, *73*, 6569.

(8) Brinckerhoff, W. B.; Morin, B. G.; Brandon, E. J.; Miller, J. S.; Epstein, A. J. *J. App. Phys.* **1996**, *79*, 6147.

(9) Summerville, D. A.; Cape, T. W.; Johnson, E. D.; Basolo, F. *Inorg. Chem.* **1978**, *17*, 3297.

(10) Wynn, C. M.; Gîrtu, M.; Brinckerhoff, W. B.; Sugiura, K.-i.; Miller, J. S.; Epstein, A. J. *Chem. Mater.* **1997**, *9*, 2156.

(11) (a) Adler, A. D.; Longo, F. R.; Finarelli, J. D.; Goldmacher, J.; Assour, J.; Korsakoff, L. *J. Org. Chem.* **1967**, *32*, 476. (b) Jones, R. D.; Summerville, D. A.; Basolo, F. *J. Am. Chem. Soc.* **1978**, *100*, 446. (c) Brandon, E. J.; Rittenberg, D. K.; Arif, A. M.; Miller, J. S. *Inorg. Chem.* **1998**, *37*, 3376.

Table 2. Summary of the Crystallographic Data for [MnTPP][TCNE]·*x*S

	S, *x*				
	PhMe, 2 (**1a**)	1,2-$C_6H_4Me_2$, 1 (**1b**)	1,2-$C_6H_4Cl_2$, 3 (**1c**)	1,3-$C_6H_4Cl_2$, 2 (**1d**)	1,2,4-$C_6H_3Cl_3$, 2 (**1e**)
formula	$C_{64}H_{44}MnN_8$	$C_{58}H_{38}MnN_8$	$C_{68}H_{40}Cl_6MnN_8$	$C_{62}H_{36}Cl_4MnN_8$	$C_{62}H_{34}Cl_6MnN_8$
fw	980.05	901.94	1236.79	1089.72	1155.04
space group	$P\bar{1}$	$P\bar{1}$	$P\bar{1}$	$P2_1/a$	$P\bar{1}$
a, Å	10.116 (1)	9.261 (3)	9.572 (5)	9.202(2)	9.588 (1)
b, Å	11.008 (1)	10.218 (2)	12.879 (7)	25.6917(8)	10.885 (9)
c, Å	12.489 (2)	13.294 (3)	12.949 (6)	10.686(3)	14.475 (1)
α, deg	108.15 (1)	98.88 (2)	92.60 (4)	90	106.912 (7)
β, deg	98.04 (1)	94.63 (2)	106.11 (4)	94.9635(17)	99.137 (7)
γ, deg	67.92(1)	110.64 (2)	104.67 (4)	90	107.511 (0)
Z	1	1	1	2	1
V, Å^3	1224.2	1150.71	1472.2	2516.90	1327.17
μ, cm^{-1}	3.07	3.212	5.47	5.26	6.01
ρ_{calcd}, g/cm^3	1.329	1.301	1.395	1.438	1.450
$R(F)^a$	0.0569	0.0392	0.0543	0.0529	0.0403
$R_w(F)^b$	0.0885	0.0571			
$R_w(F^2)^c$			0.1557	0.1088	0.0970
temp, °C	−100	−80	25	−80	25
λ, Å	0.710 73	0.710 73	0.710 73	0.710 73	0.710 73

^{a} $\sum(|F_o| - |F_c|)/\sum|F_o|$. ^{b} $\{\sum w[F_o - F_c]^2/\sum w[F_o]^2\}^{1/2}$. ^{c} $\{\sum w[F_o^2 - F_c^2]^2/\sum w[F_o^2]^2\}^{1/2}$.

$x = 2.05$. Desolvation was performed according to the α and β_o methods, and the ν_{CN} IR data are reported in Table 1.

[MnTPP][TCNE]·*x*(1,2,4-$C_6H_3Cl_3$), 1e, was prepared as described above using 42.3 mg (0.06 mmol) of Mn^{II}TPPpy and 20.3 mg (0.16 mmol) of TCNE, both dissolved in 10 mL of boiling 1,2,4-trichlorobenzene and filtered before addition. IR (cm^{-1}) at room temperature: 2195 (m), 2136 (s) for ν_{CN}. TGA/MS: 32.1% weight loss at 150 °C corresponding to $x = 2.07$. Desolvation was performed according to the α and β_d methods, and the ν_{CN} IR data are reported in Table 1. Table 1 reports the major IR peaks for the single-phase solvated crystals used for structure analysis. In a typical preparation **1e** has minor IR peaks at 2202 (vw), 2182 (w), 2162 (w), and 2146 (m) in addition to major peaks at 2195 (m) and 2136 (s). This is possibly due to rapid partial desolvation or other structural defects in the lattice.

Physical Methods. The 2−300 K dc magnetic susceptibility was determined on the equivalent of a Quantum Design MPMS-5XL 5 T SQUID as previously described.[11c] Desolvated samples were loaded in gelatin capsules, and solvated samples were loaded in an airtight Delrin holder packed with oven-dried quartz wool, and a minimal amount of solvent was added to prevent movement of the sample in the holder at low temperature when the solvent became frozen. Delrin holders were loaded and sealed within the first 2 min of filtering the solution in order to minimize solvent loss. The samples were cooled in zero applied field with data then taken upon warming. In addition to correction for the diamagnetic contribution from the sample holder, core diamagnetic corrections of −430, −60, −65.9, −77.8, −83.2, −84.3, and −106.5 × 10^{-6} emu/mol were used for MnTPP, TCNE, PhMe, 1,2-$C_6H_4Me_2$, 1,2-$C_6H_4Cl_2$, 1,3-$C_6H_4Cl_2$, and 1,2,4-$C_6H_3Cl_3$, respectively. High-field (±120 000 Oe) hysteresis experiments were performed on an Oxford Instruments vibrating sample magnetometer. Infrared spectra (±1 cm^{-1}) were obtained on a Bio-Rad FT-40 spectrophotometer in mineral oil mulls between NaCl plates. The IR spectrometer was equipped with a homemade heating system consisting of four button heaters controlled with a type K Ni−Cr vs Ni−Al thermocouple and an Omega CN76000 temperature readout to enable the measurement of the temperature dependence of the IR spectra from room temperature to 160 °C. The temperature was determined to be ca. 4.5 K cooler at the sample via a Fluke 80T IR temperature probe. The absolute temperatures are estimated to be ±3 K. The thermal properties were studied on a TA Instruments model 2050 thermogravimetric analyzer (TGA) equipped with a TA-MS Fison triple-filter quadrupole mass spectrometer to identify gaseous products with masses less than 300 amu. The TGA was located in a Vacuum Atmospheres DriLab under argon to protect air- and moisture-sensitive samples. Samples were placed in an aluminum pan and heated at 20 °C/min under a continuous 10 mL/min nitrogen flow. Elemental analyses were performed by Atlantic Microlabs, Norcross, GA.

X-ray Structure Determination. The structure of **1a** was solved with X-ray diffraction intensities collected on a Syntex R3 diffractometer using Mo Kα radiation at 173 K[7a] (Table 2). A hemisphere ($-12 \le h \le 13$; $-13 \le k \le 14$; $-16 \le l \le 0$) of intensity data was collected with $4.1° \le 2\theta \le 55.0°$, yielding a total of 5928 reflections of which 5022 were unique [3582 reflections $\ge 2\sigma(I)$]. Crystal stability was monitored by two standard reflections, which showed ≤1% variation throughout the data collection. No absorption correction was performed. These data were rerefined against the structure amplitudes, *F*, using the program SHELXL93[12a] on a Silicon Graphics Iris4d Indigo. Hydrogen atoms were located by difference Fourier mapping, and their positional and thermal parameters were refined except for the methyl hydrogens of the toluene, which were restrained to an ideal stereochemistry.

The refinement converged to an *R*(*F*) of 6.10% for data with $I > 2\sigma(I)$ and 9.25% for all data using 412 atomic parameters refined with anisotropic thermal parameters. The asymmetric unit comprises[7a] one-half [MnTPP]$^+$, one-half [TCNE]$^{\bullet-}$, and one toluene solvate. However, the difference density map (Figure 1) showed three significant peaks (0.99, 0.34, and 0.33 e$^-$/Å^3) in the same plane as the [TCNE]$^{\bullet-}$ into which a rotated minor form of [TCNE]$^{\bullet-}$ could be fit with two peaks nearly coincident with existing atoms. The model was rerefined to include an independent minor orientation's positional and isotropic thermal parameters with the sum of the occupancies constrained to unity and corresponding major and minor bond lengths and angles restrained to be the same value (Table 3).

The final model, including the minor [TCNE]$^{\bullet-}$ orientation, consists of 431 refined parameters with 10 restraints converging to an *R*(*F*) of 0.0569 for the 3584 reflections greater than $2\sigma(I)$ and 0.0885 for all 5022 reflections. The final weighting scheme used is $1/(\sigma^2(F^2) + 0.8336P)$, where $P = [\max(F^2,0) + 2F_c^2]/3$, and the final goodness of fit is 1.094. The highest features remaining in the difference synthesis, 0.20−0.28 e$^-$/Å^3, are in the bonds of the porphyrin ring. A Hamilton's *R*-factor test[12b] demonstrates that the modeled disorder is statistically significant with a probability of 99.5%.

Single crystals of **1b**−**e** were grown from their respective solvents, and their unit cells were determined on a CAD4 diffractometer using Mo Kα radiation. The crystallographic data are summarized in Table 2. Like **1a**, **1b**, **1c**, and **1e** belong to the $P\bar{1}$ space group determined from the lack of systematic absences and subsequent least-squares

(12) (a) Sheldrick, G. *SHELXL93, Program for the Refinement of Crystal Structures*; University of Göttingen: Göttingen, Germany, 1994. (b) Hamilton, W. C. *Acta Crystallogr.* **1965**, *18*, 502. The *R*-factor ratio, *R*, for the current model has $R_{b=21,f=3151} = 1.0510$ for $I > 2\sigma(I)$ and $R_{b=21,f=4589} = 1.0510$ for all data. In order for the disorder to be statistically significant, *R* must be greater than the extrapolated tabular value from the above reference, 1.0066 and 1.0042, respectively.

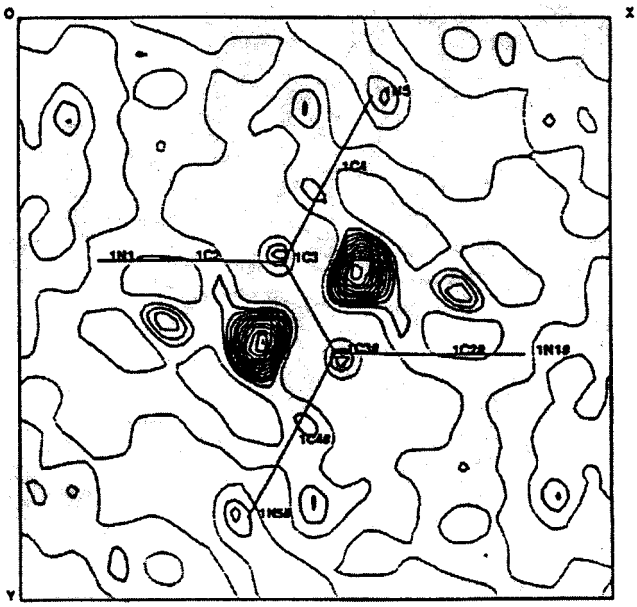

Figure 1. Difference electron density map in the plane of $[TCNE]^{\bullet-}$. Contours are at 0.1 e^- Å^3 (solid) beginning at zero e^-/Å^3.

refinement. For **1d**, the $P2_1/a$ space group was determined by the same method. During data collection the intensities of several representative reflections were measured as a check on crystal stability; there was no loss of intensity during data collection. Equivalent reflections were merged, and only those for which I_o is greater than 2 $\sigma(I)$ were included in the refinement, where $\sigma(F_o)^2$ is the standard deviation based on counting statistics. Lorentz and polarization corrections and an empirical absorption correction based on a series of ψ scans were applied to the data. Intensities of equivalent reflections were averaged. The structures were solved by the standard heavy-atom techniques with the MOLEN/VAX package. Non-hydrogen atoms were refined with anisotropic thermal parameters using SHELXL-93.[12a] The nonhydrogen atoms were refined with anisotropic displacement coefficients $U(H) = 1.2U(C)$ or $1.5U(C_{methyl})$, and their coordinates were allowed to ride on their respective carbons. The final cycle of full-matrix least-squares refinement for **1b** was based on 3003 observed reflections [$I_o > 2\sigma(I)$] and 313 parameters and converged with unweighted and weighted agreement factors $R(F) = 0.0392$ and $R_w(F) = 0.0571$, respectively. The final cycle of full-matrix least-squares refinement for **1c** was based on 3834 observed reflections [$I_o > 2\sigma(I)$] and 364 parameters and converged with unweighted and weighted agreement factors $R(F) = 0.0543$ and $R_w(F^2) = 0.1557$, respectively. The final cycle of full-matrix least-squares refinement for **1d** was based on 7968 observed reflections [$I_o > 2\sigma(I)$] and 412 parameters and converged with unweighted and weighted agreement factors $R(F) = 0.0529$ and $R_w(F^2) = 0.1088$, respectively. The final cycle of full-matrix least-squares refinement for **1e** was based on 3381 observed reflections [$I_o > 2\sigma(I)$] and 349 parameters and converged with unweighted and weighted agreement factors $R(F) = 0.0403$ and $R_w(F^2) = 0.0970$, respectively. Solvent disorder was found in **1b** and **1c**. The 1,2-xylene solvent is present in a static 50% orientational disorder for **1b**, and one of the 1,2-dichlorobenzenes is disordered evenly over an inversion center for **1c**. Disorder in any form was not observed for **1d** and **1e**. $[TCNE]^{\bullet-}$ disorder was only observed for **1a**.

Results and Discussion

Synthesis. Typical of metalloporphyrins, [MnTPP][TCNE] forms a plethora of solvates referred to as porphyrin sponges.[13] [MnTPP][TCNE]·*x*S compounds [S = PhMe, **1a** ($x = 2$); 1,2-$C_6H_4Me_2$, **1b** ($x = 1$); 1,2-$C_6H_4Cl_2$, **1c** ($x = 3$); 1,3-$C_6H_4Cl_2$, **1d** ($x = 2$); and 1,2,4-$C_6H_3Cl_3$, **1e** ($x = 2$)] were isolated from the reaction of Mn^{II}TPPpy and TCNE, with each being dissolved upon refluxing in the appropriate solvent (S) and filtered prior to reaction. A 2- to 4-fold excess of TCNE was used in each case. The products appeared as shiny black needles or plates. X-ray quality crystals were grown from solutions approximately one-tenth as concentrated as noted in the Experimental Section. In the case of 1,3-$C_6H_4Cl_2$, the starting materials were each dissolved in 5 mL of dichloromethane, filtered, and then reacted, and 1 mL of 1,3-$C_6H_4Cl_2$ was added to the resulting solution. The porphyrin sponges prefer aromatic solvents with respect to aliphatic solvents, and hence, the 1,3-$C_6H_4Cl_2$ solvate was isolated. The solvent content *x* varies with structure, and the values reported herein are determined by the structure when all solvent sites are occupied. The actual content may be less than the *x* crystallographically determined. For samples studied by magnetic susceptibility, the actual value of *x* was determined from TGA analyses and used in analyses of the data. To ensure minimal solvent loss, and hence determination of the intrinsic physical properties of the fully solvated species, all studies were performed immediately after collecting the crystals. In addition to **1a**−**e**, [MnTPP][TCNE]·*x*S, compounds with S being chlorobenzene, *m*- and *p*-xylene, mesitylene, 1,2,4-trimethylbenzene, and 1-chloronaphthalene, were also prepared, but crystals suitable for single-crystal X-ray analyses could not be obtained.[14] The magnetic properties of these materials were not studied because a structure−function relationship could not be developed.

Infrared Spectra. The ν_{CN} stretching frequencies for **1a**−**e** are 2196 ± 4 (m) and 2139 ± 10 (s) cm^{-1}. Upon desolvation the ν_{CN}'s occur at 2192 ± 1 (m) and 2134 ± 1 (s) except for desolvated **1a**, which occurs at 2147 cm^{-1} (Table 1). These values are inconsistent with $[TCNE]^0$ [2259 (s), 2221 (m) cm^{-1}], unbound $[TCNE]^{\bullet-}$ [2183 (s), 2143 (m) cm^{-1}], and $[TCNE]^{2-}$ [2104 (s), 2069 (m) cm^{-1}] [15] (Table 1). However, the solvated and desolvated materials displayed shifts in the cyano stretching frequencies with respect to unbound $[TCNE]^{\bullet-}$,[15] suggesting coordination and reduction of TCNE. Variable temperature IR (VTIR) spectra taken to 160 °C for **1a**−**e** show a ±4 cm^{-1} shift in the low-frequency cyano stretch upon heating. When **1b**−**d** are heated to 160 °C, the lowest low-frequency cyano stretch shifts to higher frequencies, while for **1a** and **1e** the high-frequency cyano stretch shifts to lower frequencies. In each case, the high-frequency cyano stretch shifts to 2189 cm^{-1} at 160

(13) (a) Goldberg, I.; Krupitsky, H.; Stein, Z.; Hsiou, Y.; Strouse, C. E. *Supramol. Chem* **1995**, *4*, 203. (b) Krupitsky, H.; Stein, Z.; Goldberg, I. *J. Inclusion Phenom. Mol. Recognit. Chem.* **1995**, *20*, 211. (c) Goldberg, I. *Mol. Cryst. Liq. Cryst.* **1996**, *278*, 767. (d) Byrn, M. P.; Curtis, C. J.; Hsiou, Y.; Kahn, S. I.; Sawin, P. A.; Tendick, S. K.; Terzis, A.; Strouse, C. E. *J. Am. Chem. Soc.* **1993**, *115*, 9480. Byrn, M. P.; Curtis, C. J.; Hsiou, Y.; Khan, S. I.; Sawin, P. A.; Terzis, A.; Strouse, C. E. *Comprehensive Supramolecular Chemistry*; Atwood, J. L., Davies, J. E. D., MacNicol, D. D., Vogtle, F., Eds.; Pergamon: New York, 1996; Vol. 6, p 715.

(14) [MnTPP][TCNE]·C_6H_5Cl. IR (cm^{-1}) at room temperature: 2197 (m), 2155 (s), and 2137 (s) for ν_{CN}. Anal. Calcd (obsd) for $C_{56}H_{33}ClN_8Mn$: C 74.05 (73.94%), H 3.66 (3.82%), N 12.34 (12.26%). [MnTPP][TCNE]·1.56(1,3-$C_6H_4Me_2$). IR (cm^{-1}) at room temperature: 2194 (m), 2147 (s), and 2138 (s) for ν_{CN}. Anal. Calcd (obsd) for $C_{62.48}H_{43.6}N_8Mn$: C 78.06 (78.00%), H 4.57 (4.74%), N 11.66 (11.66%). [MnTPP][TCNE]·0.76(1,4-$C_6H_4Me_2$). IR (cm^{-1}) at room temperature: 2192 (m) and 2134 (s) for ν_{CN}. Anal. Calcd (obsd) for $C_{56.08}H_{35.6}N_8Mn$: C 76.85 (76.43%), H 4.09 (4.37%), N 12.78 (12.51%). [MnTPP][TCNE]·0.96(1,2,4-$C_6H_3Me_3$). IR (cm^{-1}) at room temperature: 2195 (m) and 2138 (s) for ν_{CN}. Anal. Calcd (obsd) for $C_{58.64}H_{39.62}N_8Mn$: C 77.30 (76.90%), H 4.37 (4.56%), N 12.30 (12.01%). [MnTPP][TCNE]·0.32(1,3,5-$C_6H_3Me_3$). IR (cm^{-1}) at room temperature: 2196 (m), 2149 (s), and 2138 (m) for ν_{CN}. Calcd (obsd) for $C_{52.7}H_{31.6}N_8Mn$: C 76.10 (75.94%), H 3.83 (4.03%), N 13.47 (13.34%). [MnTPP][TCNE]·1.1(1-chloronaphthalene). IR (cm^{-1}) at room temperature: 2197 (m) and 2142 (s) for ν_{CN}. Calcd (obsd) for $C_{61}H_{35.7}Cl_{1.1}N_8Mn$: C 75.17 (74.77%), H 3.69 (3.81%), N 11.50 (11.54%).

(15) Dixon, D. A.; Miller, J. S. *J. Am. Chem. Soc.* **1987**, *109*, 3656.

Table 3. Summary of Key Bond Distances and Separations for [MnTPP][TCNE]·xS

	1a,[a] major orientation	**1a**,[b] minor orientation	**1b**	**1c**	**1d**	**1e**
C−C, Å	1.426(7)[c]	1.390(36)[c]	1.407(5)	1.411(8)	1.420(4)	1.395(7)
MnN_{CN}, Å	2.328(3)[d]	2.176(15)[d]	2.288(2)	2.384(4)	2.3374(16)	2.334(3)
MnNC, deg	146.8(8)[e]	152.3(39)[e]	167.0(2)	127.1(3)	121.38(14)	130.2(3)
dihedral angle, deg	55.6(3)[f]	53.9(10)[f]	82.3	29.9	28.9	36.8
MnN_{por}, Å	2.000		2.010	2.008	2.0084	2.011
Mn···Mn, Å, intrachain	10.116		10.218	9.572	9.202	9.588
Mn···Mn, Å, interchain in-registry	13.269		16.804	18.673	10.686	20.486
	14.932		19.026	20.832	13.485	22.201
			20.287	21.135	14.692	23.029
Mn···Mn, Å, interchain out-of-registry	11.006		9.261	12.879	13.645	10.885
	11.823		11.111	13.967	17.084	12.149
	13.838		16.028	17.886	17.575	16.529
	15.667		13.294	12.949		14.475
	12.498		15.446	13.803		16.043
	17.136		17.974	18.114		18.588
	18.603		15.440	16.898		14.879
	18.498		15.576	17.844		15.373
	19.047		21.046	23.265		20.860
	23.109					
	17.528					
interchain separation, Å, in-registry	13.139		16.763	18.670	10.646	20.463
interchain separation, Å, out-of-registry	10.201		8.669	12.457	12.846	10.381
	13.630		13.130	12.441	16.684	14.293
	18.979		14.642	16.657		14.323

[a] 83.3(4)%. [b] 16.7(4)%. [c] Orientation-weighted average is 1.420 Å. [d] Orientation-weighted average is 2.305 Å. [e] Orientation-weighted average is 147.9°. [f] Orientation-weighted average is 55.4°.

°C, an overall lowering of between 4 and 11 cm^{-1}. The effects observed in the VTIR are irreversible upon cooling to room temperature. As a result, desolvation was examined using either boiling octane (β_o) or dodecane (β_d) as a desolvation media. For **1a**−**e**, the high-frequency cyano stretch of the β-prepared materials are equivalent at 2192 ± 1 cm^{-1}, while the low-frequency cyano stretch for **1b**−**e** is 2134 ± 1 cm^{-1} and for **1a** is 2147 cm^{-1}. The ν_{CN} temperature dependence of **1a** was also monitored upon cooling the sample to 11 K, with only a slight reversible shift to 2148 (s) and 2196 (m) cm^{-1} being observed. Thermolysis under reduced pressure (α method) produced materials with physical properties nearly identical to those obtained via heating to reflux in *n*-octane (β method), and therefore, they were deemed to be the same β-phase materials. In contrast, different phases were observed for [MnTClPP][TCNE] [H_2TClPP = *meso*-tetrakis(4-chlorophenyl)porphyrin].[11c] While the high- and low-frequency ν_{CN} absorptions of **1d** are respectively greater and less than those for **1a**−**c** and **1e**, the ν_{CN} absorptions for the desolvated materials are equivalent (±2 cm^{-1}) to those of the desolvated materials for **1b**−**e**. **1a** exhibits a shift in the higher ν_{CN} absorption from 2195 to 2192.5 cm^{-1} for solvated and desolvated materials, respectively, while the low ν_{CN} remains unchanged. The lower frequency ν_{CN} absorptions are indicative of stronger back-bonding to Mn^{III} and Mn^{III}−N≡C bonding. Therefore, the frequency shifts are attributed to an intrachain structural rearrangement accompanied by the loss of solvent, which would decrease or increase Mn···Mn intrachain separation and thereby decrease or increase the MnNC angle and the dihedral angle formed from the [TCNE]$^{\bullet-}$ and MnN_4 mean planes. Verification of this requires structural information on the desolvated materials, which has been elusive. Thus, attempts to identify a correlation between the ν_{CN} absorptions and the magnetic properties were unsuccessful.

TGA/MS. Thermogravimetric analysis (TGA) of solvated materials showed a rapid loss of solvent in the range 100−165 °C, which was confirmed by the appearance of each solvent in the mass spectrum. In the materials in which solvent loss occurred above the boiling point of *n*-octane (bp 127 °C), the β_d method was carried out by refluxing in *n*-dodecane (bp 216 °C). A second weight loss above 300 °C is attributed to the decomposition of [TCNE]$^{\bullet-}$ based on characteristic TCNE fragments, e.g., $(CN)_2CC$ (76 amu), $(CN)_2C$ (64 amu), and $(CN)_2$ (52 amu) observed in the mass spectrum. For **1b**, **1d**, and **1e** where the solvent content determined from TGA slightly exceeded the value of 2.00 determined from single-crystal X-ray diffraction studies, the differences are ascribed to weighing errors of the small samples used in the TGA studies. A typical TGA plot for **1d** is shown in Figure 2.

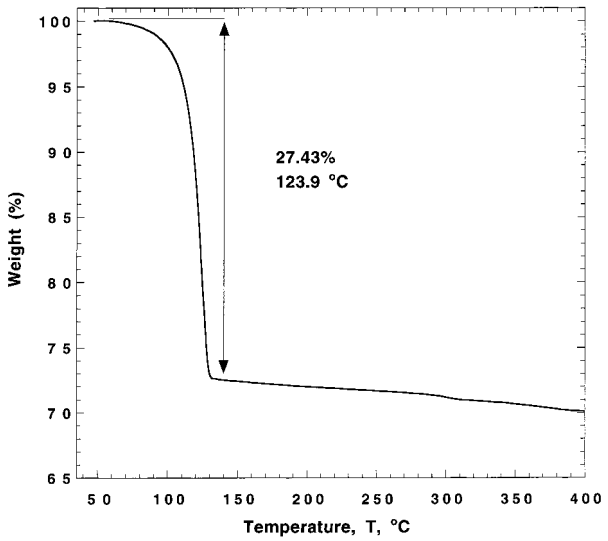

Figure 2. Thermogravimetric analysis plots of [MnTPP][TCNE]·x(1,3-$C_6H_4Cl_2$), **1d**, revealing $x = 2.05$.

Structure. The structures of **1a**−**e** were determined by single-crystal X-ray analyses, and their unit cell and metrical parameters are summarized in Table 2. Although not isomorphous, compounds **1a**−**c** and **e** are structurally similar to each, belonging to the $P\bar{1}$ space group with $Z = 1$. **1d**, in contrast, belongs to the $P2_1/a$ space group with $Z = 2$. The $P\bar{1}$ space group has been observed for most members of the [Mn-

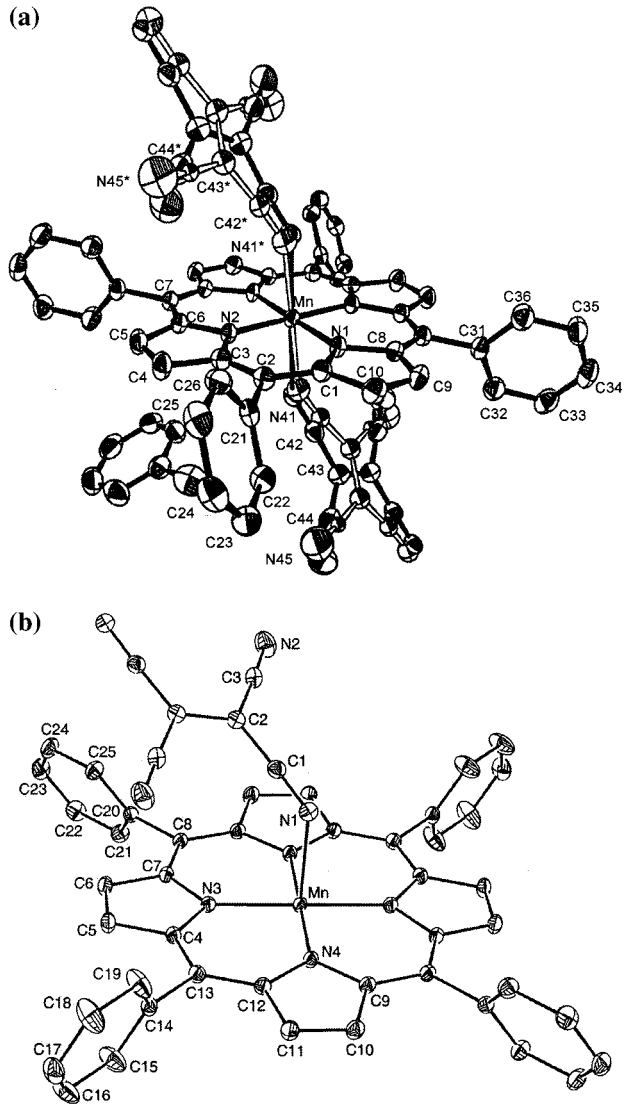

Figure 3. (a) ORTEP labeling diagram (30%) of [MnTPP][TCNE]·2PhMe, **1a**. The $[TCNE]^{\bullet-}$ minor form is shown in hollow bonds, while the major form is shown in solid bonds. (b) ORTEP labeling diagram (30%) of [MnTPP][TCNE]·2(1,3-$C_6H_4Cl_2$), **1d**. The solvents have been omitted for clarity.

(porphyrin)][TCNE]·*x*S family; however, $P2_1/a$ has been observed for [MnTXPP][TCNE]·2(CH_2Cl_2) (X = Cl,[11c] Br[17]) and [$MnTF_4$OMePP][TCNE]·2PhMe[18] [H_2TF_4OMePP = tetrakis-(2,3,5,6-tetrafluoro-4-methoxyphenyl)porphyrin].

The structures of the $[MnTPP]^+$ cations are indistinguishable and consistent with other related $[MnTPP]^+$ cations in the literature.[3a,7a,11c,13,17−21] In each case the $[MnTPP]^+$ cation is planar with a $MnN_{pyrrole}$ bond distance of 2.007 ± 0.008 Å. The intramolecular $[TCNE]^{\bullet-}$ bond distances and angles are indistinguishable from each other and to related compounds.[4b,15,17−20] The central CC bonds are 1.41 ± 0.01 Å, consistent with a bond order of 1.5 as expected for $[TCNE]^{\bullet-}$.[15]

Solvent fills the cavities between the parallel chains, and it is anticipated that desolvation would allow a collapse of the intrachain stacking and/or a decrease in interchain separation.[13]

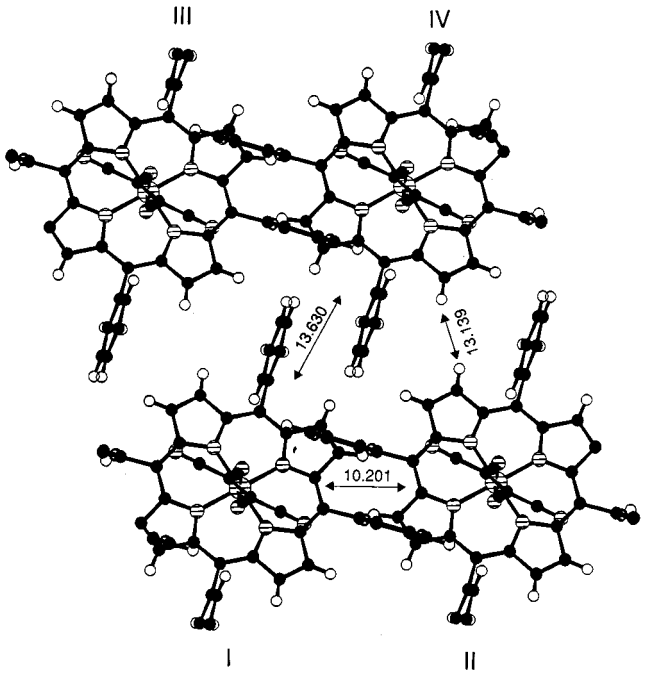

Figure 4. View down the *a* axis normal to the parallel chains, showing the interchain interactions between chains **I**, **II**, **III**, and **IV** for [[MnTPP][TCNE]·2PhMe, **1a**.

The important inter- and intrachain distances and angles are listed in Table 3. The intrachain Mn···Mn separation is the greatest for **1b** at 10.218 Å and least for **1d** at 9.202 Å, and these two separations are associated with the largest and smallest $[TCNE]^{\bullet-}$−MnN_4 dihedral angles (82.3° and 28.9°) and $MnNC_{TCNE}$ angles (167.0 and 121.4°), respectively. The in-registry, interchain Mn···Mn separations range from 10.646 to 20.486 Å.

The ORTEP atom-labeling diagram for **1a** is presented in Figure 3a, while the ORTEP atom-labeling diagram for **1d** (and **1b** and **1c**) is presented in Figure 3b. For **1a**−**e** the $[TCNE]^{\bullet-}$ is uniformly trans-μ-*N*-σ-bound to two Mn^{III}'s forming parallel 1-D ···$D^+A^{\bullet-}D^+A^{\bullet-}$··· (D = MnTPP; A = TCNE) chains along the crystallographic *a* axis for **1a** and **1c**−**e** and along the *b* axis for **1b**. The chains of **1a (1b**, **1c**, **1e)** lie parallel to each other (Figure 4), with contacts between chains **I**−**II**, **I**−**III**, and **I**−**IV**. Chains **I**−**II** and **I**−**IV** are out-of-registry, while chains **I**−**III** are in-registry**.** The key inter- and intrachain interactions can be found in Figure 5 and Table 3. Compounds **1b**, **1c**, and **1e** are structurally similar, and their important intra- and interchain separations are summarized in Table 3. The parallel chains of **1d** exhibit the closest contacts between chains **I**−**II**, **I**−**III**, **II**−**III**, and **I**−**IV** (Figure 6). The presence of a mirror plane between the two porphyrins in the unit cell results in in-registry and a herringbone arrangement of chains **I**−**III**, while **I**−**II** and **I**−**IV** (=**II**−**III**) are out-of-registry (Figure 7). The shortest in-registry interchain Mn···Mn separations range from 10.686 (**1d**) to 13.269 Å (**1a**), while the shortest out-of-registry interchain Mn···Mn separations range from 9.261 (**1b**) to 13.645 Å (**1d**) for **1a**−**e**. Starting from an imaginary line through the Mn's within a chain, the interchain separations for the in-registry chains range from 10.646 (**1d**) to 20.463 Å (**1e**) and the out-of-registry separation range from 8.669 (**1b**) to 12.846 Å (**1d**). For **1a**−**c**,**e** with the $P\bar{1}$ space group the shortest interchain separation lies between out-of-registry chains. However, for **1d** with the $P2_1/a$ space group, the shortest interchain separation is between the in-registry chains. Additional distances and angles are summarized in Table 3.

(16) Brandon, E. J.; Kollmar, C.; Miller, J. S. *J. Am. Chem. Soc.* **1998**, *120*, 1822.
(17) Rittenberg, D. K.; Sugiura, K.-i.; Sakata, Y.; Mikami, S.; Epstein, A. J.; Miller, J. S. *Adv. Mater.* **2000**, *12*, 126.
(18) Rittenberg, D. K.; Sugiura, K.-i.; Sakata, Y.; Guzei, I. A.; Rheingold, A. L.; Miller, J. S. *Chem.—Eur. J.* **1999**, *5*, 1874.

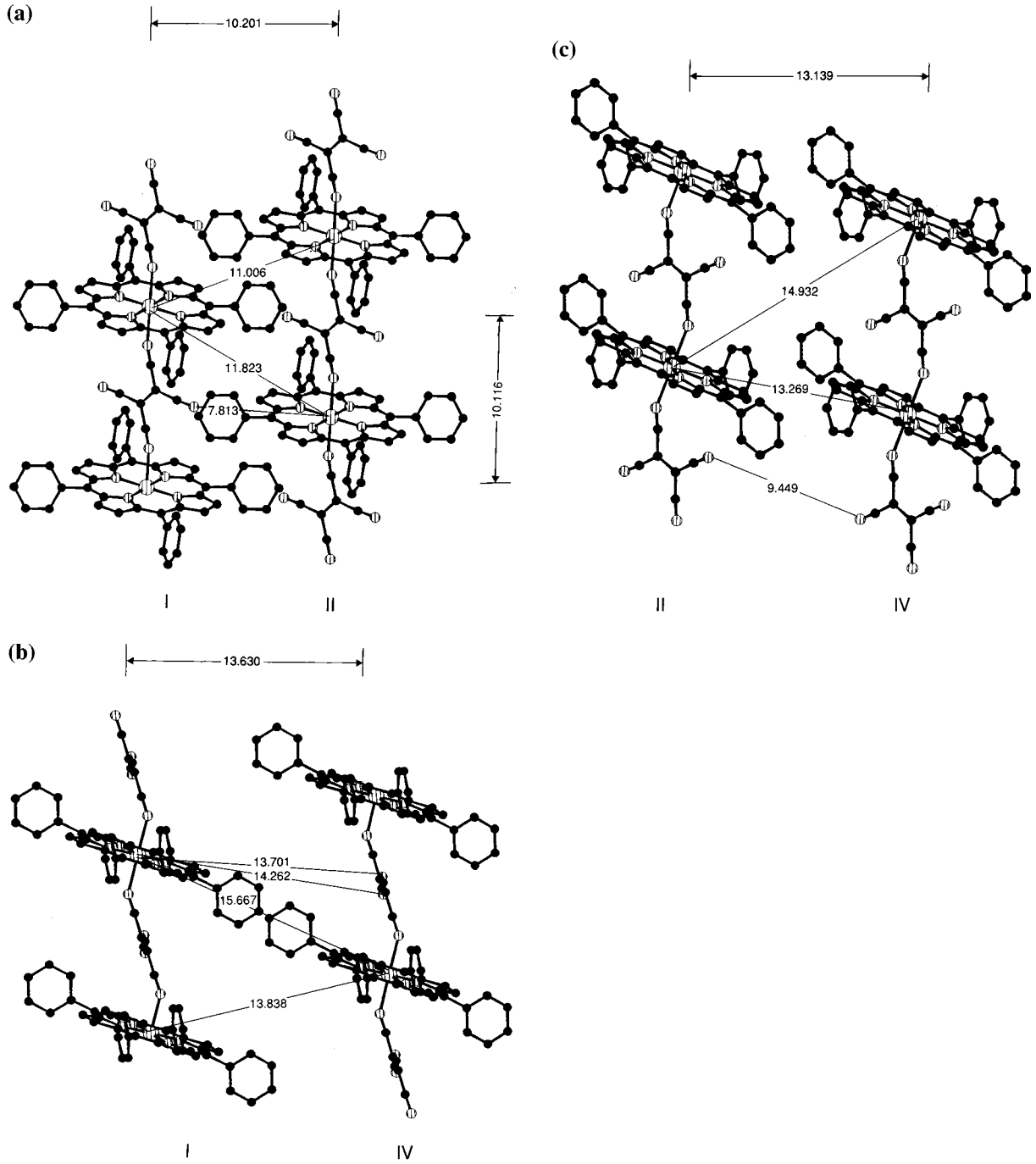

Figure 5. View parallel to out-of-registry chains **I**−**II** (a) and **I**−**IV** (b) and in-registry chains **I**−**III** (c) [MnTPP][TCNE]·2PhMe, **1a**.

Disorder in the orientation of [TCNE]^{0} has been observed for several electron and charge-transfer complexes[22] in which the [TCNE]^{0} lies between donors, thereby maximizing the overlapping electron orbitals. Because [TCNE]^{0} and [TCNE]$^{\bullet-}$ are nearly square (4.06 Å × 4.39 Å), the disorder can be described as (i) an approximate 180° rotation about the central CC bond or (ii) a 90° rotation about an axis perpendicular to the TCNE plane, passing through the center of the TCNE molecule. Disorder for [TCNE]$^{\bullet-}$ is not well documented, but should be identical to that reported for TCNE, and may be expected to occur when either TCNE or [TCNE]$^{\bullet-}$ is trans-μ-bound to metal ions. The preservation of the metal coordination, as observed for **1a**, supports that the rotation is best described as an approximate 180° rotation about the central CC bond.

[TCNE]$^{\bullet-}$ is 2-fold orientationally disordered in the structure of [MnTPP][TCNE]·2PhMe, **1a** (Figure 3a). The major form (filled bonds) has a refined occupancy of 83.3(4)%, while the minor form (hollow bonds) has an occupancy of 16.7(4)%. The central CC bond is 1.426(7) and 1.390(36) Å, respectively, for the major and minor orientations characteristic of a 1.5 bond

(19) (a) Böhm, A.; Vazquez, C.; McLean, R. S.; Calabrese, J. C.; Kalm, S. E.; Manson, J. L.; Epstein, A. J.; Miller, J. S. *Inorg. Chem.* **1996**, *35*, 3083. (b) Sugiura, K.-i.; Arif, A.; Rittenberg, D. K.; Schweizer, J.; Öhrstrom, L.; Epstein, A. J.; Miller, J. S.; *Chem.—Eur. J.* **1997**, *3*, 138.

(20) (a) Brandon, E. J.; Sugiura, K.-i.; Arif, A. M.; Liable-Sands, A.; Rheingold, A. L.; Miller, J. S. *Mol. Cryst. Liq. Cryst.* **1997**, *305*, 269. (b) Brandon, E. J.; Burkhart, B. M.; Rogers, R. D.; Miller, J. S. *Chem.—Eur. J.* **1998**, *4*, 1938. (c) Brandon, E. J.; Arif, A. M.; Burkhart, B. M.; Miller, J. S. *Inorg. Chem.* **1998**, *37*, 2792. (d) Brandon, E. J.; Arif, A. M.; Miller, J. S.; Sugiura, K.-i.; Burkhart, B. M. *Crystal Eng.* **1998**, *1*, 97. (e) Sugiura, K.-i.; Mikami, S.; Tanaka, T.; Sawada, M.; Manson, J. L.; Miller, J. S.; Sakata, Y. *Chem. Lett.* **1997**, 1071.

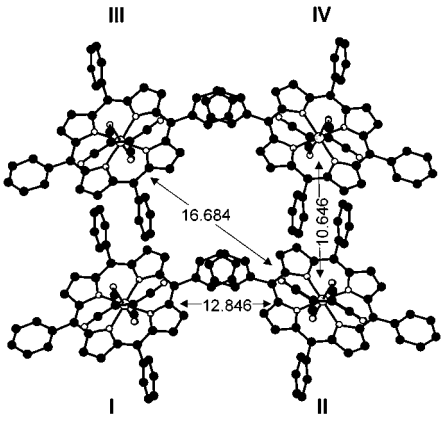

Figure 6. View down the *a* axis normal to the parallel chains, showing the interchain interactions between chains **I**, **II**, **III**, and **IV** for [MnTPP][TCNE]·2(1,3-$C_6H_4Cl_2$), **1d**.

order and assignment of $[TCNE]^{\bullet-}$.[15] The major and minor $[TCNE]^{\bullet-}$ orientations have MnN distances of 2.328(3) and 2.176 (15) Å and a MnNC angle of 146.8(8)° and 152.3(39)° for the major and minor orientations, respectively. Hence, the orientation-weighted average distance and angle are 2.305 Å and 147.9°, respectively. The dihedral angle between the MnN_4 and the major and minor $[TCNE]^{\bullet-}$ orientation mean planes are 55.6(3)° and 53.9(10)°, respectively, and the orientation-weighted average dihedral angle is 55.4°. These Mn−N distances are comparable to those of other structures[3a,7a,11c,17−20] and consistent with that of a high-spin six-coordinated Mn^{III}.

Magnetic Data. The 2−300 K magnetic susceptibility was determined for **1a**−**e** and their α and *β* desolvated phases, and the data are summarized in Table 4. The 300 K effective moments range from 4.3 to 5.5 μ_B, averaging 4.8 μ_B. Values less that 5.20 μ_B are due to antiferromagnetic coupling evident at room temperature, while values higher than 5.20 μ_B are likely due to errors in molecular weight due to the specific degree of solvation, or conversely, a consequence of interchain coupling, strong coupling with $T_{min} \gg 300$ K (Table 4). The susceptibilities of **1a** **1a**-α, and **1a**-*β* can be fit to a Curie−Weiss expression χ [$\propto 1/(T - \theta)$] in two linear regions. The data above ∼250 K for **1a** and >200 K for **1a**-α and **1a**-*β* were fit with θ values of −267, −123, and −40 K for **1a**, **1a**-α, and **1a**-*β*, respectively, indicative of dominant antiferromagnetic coupling. Below ∼200 K the data can be fit with effective θ (θ')[11c] values of 44, 41, and 49 K, respectively, indicative of longer range ferromagnetic coupling. Likewise, **1b**-α (and **1b**-*β*) has θ and θ' values of −16 (−20) and 40 (52 K), respectively. The susceptibility of the remaining 10 compounds, as typified by [MnTPP][TCNE]·*x*(1,3-$C_6H_4Cl_2$), **1d** (Figure 8), can be fit only in one region

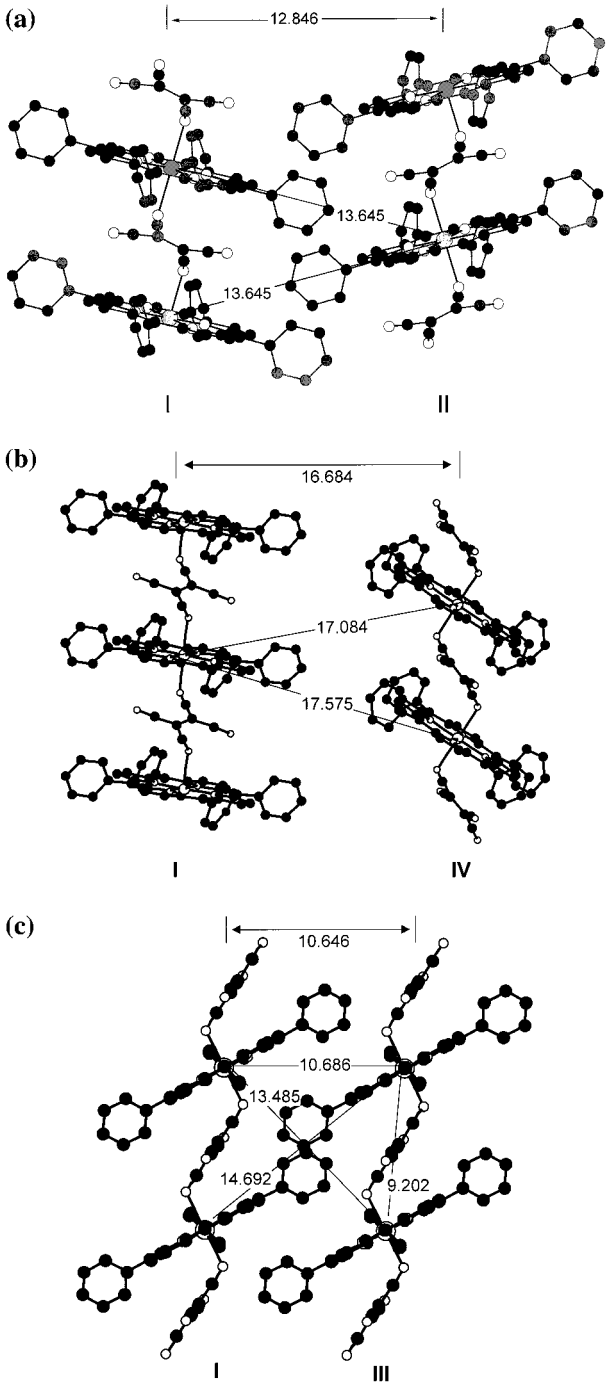

Figure 7. View parallel to out-of-registry chains **I**−**II** (a) and **I**−**IV** **(II**−**III)** (b) and in-registry chains **I**−**III** (c) for MnTPP][TCNE]·2(1,3-$C_6H_4Cl_2$), **1d**.

with θ' ranging from 44 (**1a**) to 104 K (**1e**-*β*), indicative of stronger 2-D and 3-D ferromagnetic coupling. The θ' values for **1d** can be enhanced by as much as 58% upon desolvation. However, decreases in θ' values were observed for **1b**-α and **1b**-*β*. Hence, thermolysis can either increase or decrease the magnitude of the θ' values. Minima in the $\chi T(T)$, i.e., T_{min}, are observed for **1***x*, **1***x*-α, and **1***x*-*β* (*x* = **a**, **b**) between 191 and 292 K, again indicating dominant antiferromagnetic coupling.[23] **1d** has a T_{min} at 275 K, and the remaining solvated and desolvated materials did not display a T_{min} within the measured temperature range, but T_{min} is expected to occur above 300 K and is estimated by the Seiden expression (vide infra).

The 1-D intrachain coupling, J_{intra}, of the [MnTPP][TCNE] series was determined from modeling $\chi T(T)$ with the Seiden[24]

(21) (a) Day, V. W.; Sults, B. R.; Tasset, E. L.; Marianelli, R. S.; Boucher, L. J. *Inorg. Nucl. Chem. Lett.* **1975**, *11*, 505. (b) Cheng, B.; Cukiernik, F.; Fries, P.; Marchon, J.-C.; Scheidt, W. R. *Inorg. Chem.* **1995**, *34*, 4627. (c) Guildard, R.; Perie, K.; Barbe, J.-M.; Nurco, D. J.; Smith, K. M.; Caemelbecke, E. V.; Kadish, K. M. *Inorg. Chem.* **1998**, *37*, 973. (d) Landrum, J. T.; Hatano, K.; Scheidt, W. R.; Reed, C. A. *J. Am. Chem. Soc.* **1980**, *102*, 6729. (e) Hill, C. L.; Williamson, M. M. *Inorg. Chem.* **1985**, *24*, 3024. (f) Fleischer, E. B. *Acc. Chem. Res.* **1970**, *3*, 105. (g) Scheidt, W. R.; Reed, C. A. *Chem. Rev.* **1981**, *81*, 543. (h) Turner, P.; Gunter, M. J.; Hambley, T. W.; White, A. H.; Skelton, B. W. *Inorg. Chem.* **1992**, *31*, 2297.

(22) (a) Saheki, M.; Yamada, H.; Yoshioka, H.; Nakatsu, K. *Acta Crystallogr., Sect. B* **1976**, *32*, 662. (b) Maverick, E.; Trueblood, K. N.; Bekoe, D. A. *Acta Crystallogr., Sect. B* **1978**, *34*, 2777. (c) Larsen, F. K.; Little, R. G.; Coppens, P. *Acta Crystallogr., Sect. B* **1975**, *31*, 430. (d) Bernstein, J.; Trueblood, K. N. *Acta Crystallogr., Sect. B* **1971**, *27*, 2078. (e) Lee, D.; Wallwork, S. C. *Acta Crystallogr., Sect. B* **1978**, *34*, 3604. (f) Renault, A.; Cohen-Addad, C. *Acta Crystallogr., Sect. C* **1986**, *42*, 1529.

Table 4. Summary of Magnetic Properties for [MnTPP][TCNE]·*x*S

	μ_{eff}, μ_B	θ, K	θ', K	T_{min}, K	J_{intra}, K[a]	T_c,[b] K	ϕ[b]	χ'' [b]	H_c (2 K), kOe	M(2K,5T), emu Oe/mol
1a	4.65	−267	44	191	−63	7.8[e]	0.167	6.4	22.9	14 600
1a-α	4.97	−123	41	195	−65	11.1[e]	0.109	8.9	23.2	16 100
1a-β	4.72	−40	49	263	−88	11.7[e]	0.103	9.6	22.4	11 940
1b	4.30	[c]	52	292	−99	9.2	0.168	7.9	25.4	12 300
1b-α	4.92	−16	40	247	−86	11.6	0.099	9.1	22.3	11 500
1b-β	4.86	−20	52	276	−99	15.3	0.003	11.3	22.6	12 700
1c	5.28	[c]	72	700[d]	−234	11.3	0.066	8.1	25.6	15 750
1c-α	4.80	[c]	75	720[d]	−240	9.5	0.170	8.2	27.0	13 800
1c-β	5.05	[c]	74	625[d]	−210	9.8	0.151	8.4	26.6	12 200
1d	5.50	[c]	55	275	−100	10.8	0.171	8.8	26.8	11 800
1d-α	4.90	[c]	75	650[d]	−217	9.5	0.16	8.3	26.5	12 000
1d-β	4.65	[c]	87	880[d]	−295	9.7	0.157	8.6	26.8	11 800
1e	4.50	[c]	77	600[d]	−200	8.2[f]	0.024	6.6	26.5	13 000
1e-α	4.79	[c]	74	750[d]	−250	9.4	0.17	8.1	27.0	11 800
1e-β	4.32	[c]	104	1080[d]	−360	9.4	0.181	8.3	27.1	11 300

[a] Based on best fit of the Seiden model ($H = -2J\mathbf{S_a}\cdot\mathbf{S_b}$). [b] Temperature at which $\chi''(T)$ at 10 Hz is at its maximal value. [c] Not observed. [d] Determined from the Seiden model (see text). [e] Reported as $M(T)$, $M \rightarrow 0$, $T_c = 23$, 24, 25 K, respectively, for **1a**, **1a**-α, and **1a**-β at 1000 G field. [f] An additional peak is observed at 9.4 K attributed to the presence of a desolvated phase.

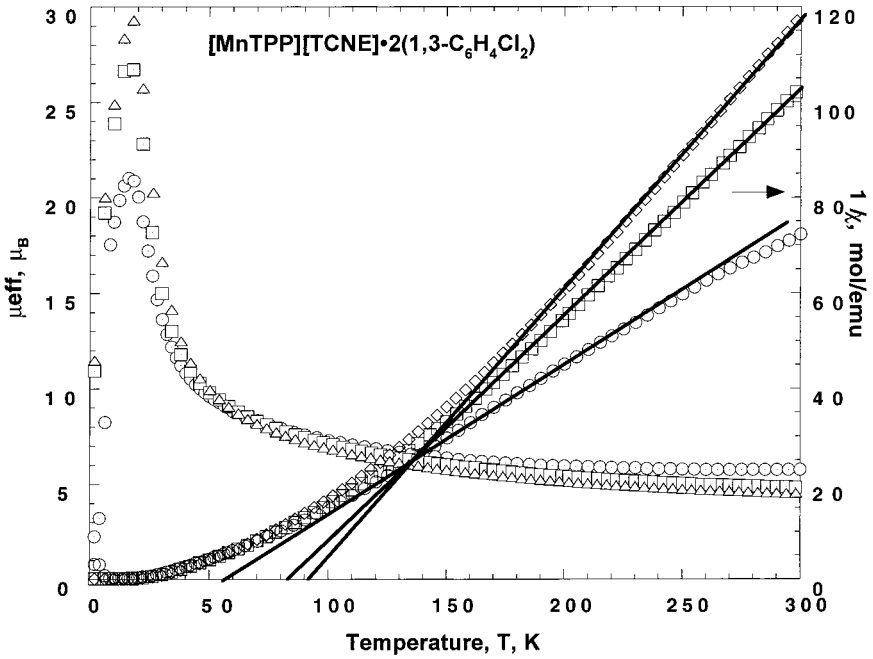

Figure 8. Magnetic moment μ_{eff} and inverse susceptibility χ^{-1} as a function of temperature for [MnTPP][TCNE]·2(1,3-$C_6H_4Cl_2$), **1d**, showing μ_{eff} values of 5.50 (●), 4.90 (⊡), and 4.65 (Δ) μ_B and θ values of 55 (○), 75 (□) and 87 (◇) K, respectively, for **1d**, **1d**-α, and **1d**-β.

expression, assuming $H = -2J\mathbf{S_a}\cdot\mathbf{S_b}$ and $g = 2$. These observed negative J_{intra}/k_B values of −63, −99, −234, −100 (Figure 9), and −200 K for **1a**−**e**, respectively (Table 4), are indicative of antiferromagnetic coupling. Upon thermolysis the θ' values and J_{intra} increase for **1d** and **1e** but in general may either increase or decrease as noted for **1a**−**c** (Table 4). In cases where T_{min} could not be observed, it was estimated from a fit to the Seiden model and ranges from 625 (**1c**-β) to 1080 K (**1e**-β) (Figure 9).

The Seiden model may not be valid for temperatures below ca. 50 K because of increased 3-D spin correlations or for systems in which the intrachain coupling is weak, likely because of next-nearest-neighbor interactions. **1a**-α, **1a**-β, **1b**, and **1b**-α deviations from the Seiden model occur below 150 K. The shape and position of the minimum in $\chi T(T)$, when present, was modeled to estimate J_{intra} from the Seiden expression. The coupling of the [TCNE]$^{\bullet-}$ with Mn^{III} is antiferromagnetic, $J_{intra} < 0$, because of direct exchange. Although an inverse correlation between θ' and either the $MnNC_{TCNE}$ angle or the MnN_4 and [TCNE]$^{\bullet-}$ mean plane dihedral angle has been proposed for several ditoluene solvates of aryl-substituted [MnTPP][TCNE]'s,[16] this correlation does not exist for this group of materials in which only the solvents are altered.

Isothermal field-dependent magnetization experiments reveal magnetizations at 50 kOe at either 2 or 5 K in the range 11 300 (**1e**-β) to 16 100 (**1a**-α) emu Oe/mol (Table 4). For an antiferromagnetic $S_{tot} = 2 - {}^1/_2 = {}^3/_2$ system, the expected saturation magnetization M_s is 16 755 emu Oe/mol, and for a ferromagnetic $S_{tot} = 2 + {}^1/_2 = {}^5/_2$ system, M_s is expected to be 27 925 emu Oe/mol. The magnitude of the magnetization at 5 T is lower than expected for an antiferromagnetically coupled $S = 2 - {}^1/_2$ system; however, on the basis of the slope of the

(23) (a) Coronado, E.; Drillon, M.; Georges, R. In *Research Frontiers in Magnetochemistry*; O'Connor, C. J., Ed.; World Scientific: Singapore, 1993; p 26. (b) Beltran, D.; Coronado, E.; Drillon, M.; Georges, R. *Stud. Inorg. Chem.* **1983**, *3*, 583. (c) Drillon, M.; Coronado, E.; Beltran, D.; Georges, R. *Chem. Phys.* **1983**, *79*, 449. (d) Verdaguer, M.; Julve, M.; Michalowicz, A.; Kahn, O. *Inorg. Chem.* **1983**, *22*, 2624. (e) Drillon, M.; Gianduzzo, J. C.; Georges, R. *Phys. Lett.* **1983**, *96A*, 413.
(24) Seiden, J. *J. Phys. Lett.* **1983**, *44*, L947.

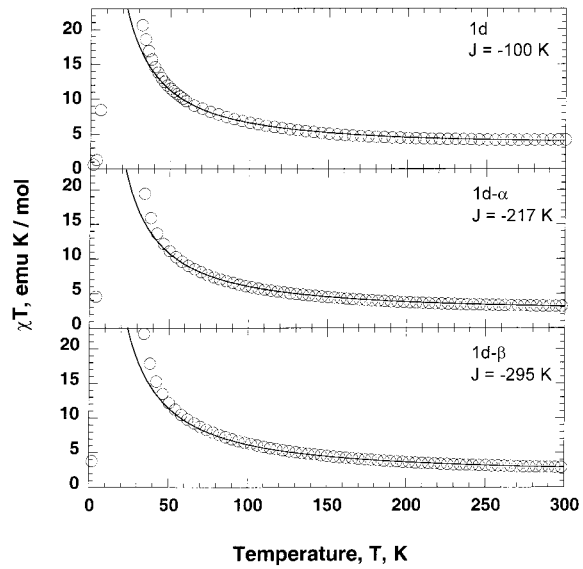

Figure 9. Seiden model fit to the $\chi T(T)$ data $[MnTPP]^+[TCNE]^{\bullet-}\cdot 2(1,3\text{-}C_6H_4Cl_2)$ and the desolvated phases with $J_{intra} = -100$, -217, -295 K for **1d**, **1d**-α, and **1d**-β, respectively ($H = -2J\mathbf{S_a}\cdot\mathbf{S_b}$).

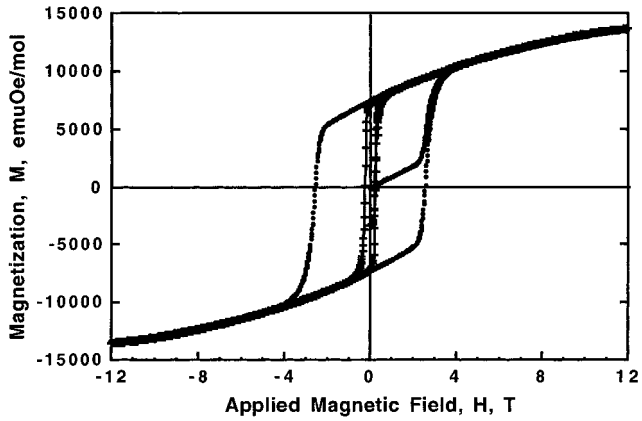

Figure 10. Magnetization as a function of field (±12 T) at 2 (●) and 5 (+) K for α-[MnTPP][TCNE], **1e**-α.

$M(H)$ curves, saturation was not evident. On the basis of the magnitude of M, these materials are ferrimagnets.[7b] Unlike at 5 K, the 2 K $M(H)$ rises gradually with increasing applied field before rising more rapidly in a manner typical of a metamagnet with a large critical field H_c. Critical fields range from 22.9 to 26.8 kOe for **1a**−**e** and range from 22.3 to 27.1 kOe for desolvated **1a**−**e** (Table 4). The genesis of this behavior is the subject of ongoing studies[17] and is representative of complex competing magnetic behaviors being present in this class of materials.

The $M(H)$ for **1e**-α was measured to ±120 kOe, and even at this high-applied magnetic field **1e**-α did not saturate (Figure 10). [For this experiment on a different instrument, even at 120 kOe, its magnetization was 13 450 emu Oe/mol, which is 80% of expectation.] The H_c for **1e**-α is 26.0 kOe. The low magnetization at high field and the lack of saturation is attributed to canting and spin glass behavior (vide infra).

Magnetic ordering temperatures T_c for **1a**−**e** were determined by the initial peak in the in-phase susceptibility at 10 Hz, $\chi'(T)$. T_c ranges from 7.8 to 11.3 K for **1a**−**e**, with the 1,2-dichlorobenzene-solvate (**1c**) having the greatest T_c. The 10 Hz peak for **1d** at 10.8 K decreases to 9.5 and 9.7 (~11% decrease) upon α and β desolvation, respectively, with similar effects observed for **1c**. The 10 Hz peak for **1a** increases by an average of 45% upon desolvation, shifting from 7.8 K to 11.1 and 11.7 K for the α and β forms, respectively, with similar results seen for **1b**,**c**.

T_c for **1a** was previously reported as ~13 K, using a scaling analysis with the additional reporting of a "shoulder" at ~7 K, which was explained as typical "reentrant" spin glass behavior.[8] Solvated **1a** has a T_c of 7.8 K; however, desolvation increases T_c to 11.4 ± 0.3 K. Hence, the earlier report of $T_c \approx 13$ K and a shoulder at ~7 K is now attributed to the presence of solvated, partially solvated, and desolvated **1a**. Although the magnetic behavior of solvated and desolvated phases are reported herein, the magnetic behavior of partially solvated phases was not specifically studied. In contrast to **1a**, the T_c of **1c**−**d** decreased upon desolvation and the T_c for **1b**,**e** increased upon desolvation. Thus, the change in magnetic behavior upon desolvation cannot be predicted a priori. **1e** has two peaks in $\chi'(T)$, with the higher temperature peak occurring at the same temperature as both the α and β desolvates. Therefore, the multiphase behavior is suspected to be a result of partial desolvation or a phase change. The T_c reported in Table 4 is that represented by the lower temperature peak, 8.2 K, because it is uncharacteristic of either the α or β desolvates. Each reported $\chi'(T)$ peak is associated with a $\chi''(T)$ peak consistent with a ferrimagnetic state as observed for [MnOEP][MnTPP][$C_4(CN)_6$] (H_2OEP = octaethylporphyrin).[10,25] These peaks range from 6.4 (**1a**) to 11.3 K (**1b**-β). Frequency (ω) dependencies of the ac susceptibility, $\phi = \Delta T_f/(T_f\, \Delta\log\, \omega)$, for the solvates range from 0.035 to 0.171, consistent with typical spin glasses[26] as reported for related materials.[4a,20] Very small ϕ values (<0.001) are typically noted for ferromagnets and weak ferromagnets. However, disordered spins systems display ϕ values that typically range from 0.01 to 0.1 such as those found in the alloys of *Pd*Mn, $\phi = 0.013$, and *Ni*Mn, $\phi = 0.018$, and the superparamagnet a-(Ho_2O_3)-(B_2O_3), $\phi = 0.28$.[26] One source of spin glass behavior is disorder,[26] and as noted earlier, although $[TCNE]^{\bullet-}$ is disordered in **1a**, magnets not exhibiting structural disorder also exhibit spin glass behavior. Hence, the genesis of spin glass behavior for this family of magnets is still under study.

Magnetic ordering is also evident by the presence of hysteresis loop. **1d** has a high coercive field, H_{cr}, of 25.6 kOe at 2 K and a remanent magnetization of 7380 emu Oe/mol, typical for [Mn(porphyrin)][TCNE] systems.[17] (At 5 K, H_{cr} is 2300 kOe and the remanent magnetization is 7150 emu Oe/mol.) In addition to hysteresis, these materials show metamagnetic-like behavior such that above a metamagnetic-like critical field H_c (Table 4) the exchange pathways are sufficient to sustain spin alignment. This interesting effect is the subject of ongoing studies.[17]

A relationship between structure and magnetic properties continues to be elusive. The data herein and that previously reported[3a,16] demonstrate a trend toward higher θ' being associated with a smaller dihedral angle formed from the $[TCNE]^{\bullet-}$ and MnN_4 mean planes. These angles are influenced by the size of the solvent molecule or the porphyrin ring substituents. The Mn···Mn distances are the closest in **1c**−**e**, which have large chlorinated solvents. In these cases, space is made for these solvents through larger interchain distances. **1d**, however, does not follow this trend, having a lower than expected θ', 55 K,

(25) Wynn, C. M.; Gîrtu, M.; Miller, J. S.; Epstein, A. J. *Phys. Rev.* **1997**, *B56*, 14050. Wynn, C. M.; Gîrtu, M.; Miller, J. S.; Epstein, A. J. *Phys. Rev. B.* **1997**, *56*, 315.

(26) Mydosh, J. *Spin Glasses: An Experimental Introduction*; Taylor and Francois: London, 1993; pp 64−76.

for its small dihedral angle of 28.9°. This may be due to the unique space group of **1d**, $P2_1/a$, compared to the $P\bar{1}$ space group of **1a**−**c,e**.

Acknowledgment. The authors appreciate the constructive comments and insight provided by E. J. Brandon, C. M. Wynn, and M. Gîrtu. We also thank J. L. Manson for high-field hysteresis experiments performed in collaboration with Oxford Instruments, using a 12 T MagLab vibrating sample magnetometer. We also gratefully acknowledge the support in part from the National Science Foundation, Grants CHE9320478 and CHE9730984. K.-i.S. also acknowledges support from the Monbu-sho fellowship program (Monbu-sho is the Ministry of Education, Science and Culture, Japan).

Supporting Information Available: A summary of the crystallographic data, tables of fractional coordinates and isotropic thermal parameters, anisotropic thermal parameters, bond distances and angles for [MnTPP][TCNE]·xS = PhMe (x = 2) (**1a**), 1,2-$C_6H_4Me_2$ (x = 1) (**1b**), 1,2-$C_6H_4Cl_2$ (x = 3) (**1c**), 1,2,4-$C_6H_3Cl_3$ (x = 2) (**1d**), and 1,3-$C_6H_4Cl_2$ (x = 2) (**1e**). This material is available free of charge via the Internet at http://pubs.acs.org.

IC0011922